Orbital alignment in atoms generated by photodetachment in a strong laser field

Mikael Eklund,[1] Hannes Hultgren,[1] Dag Hanstorp,[2] and Igor Yu. Kiyan[1,*]
[1]*Physikalisches Institut, Albert-Ludwigs-Universität, 79104 Freiburg, Germany*
[2]*Department of Physics, University of Gothenburg, SE-412 96 Gothenburg, Sweden*
(Received 2 July 2013; published 26 August 2013)

A pump-probe laser scheme is employed to investigate orbital alignment and its dynamics in the ground state of laser-generated neutral atoms. The alignment is initiated by electron photodetachment of an atomic negative ion in a strong laser pulse. The electron density distribution in the ground state of the residual atom is probed by means of strong-field ionization in a second laser pulse at a delayed time. The principle of the probe method relies on the fact that the portion of the electron density distribution oriented along the laser polarization axis constitutes the ionization yield in the high-energy jets of emitted electrons. A systematic study is carried out on C, Si, and Ge atoms, which possess two electrons in an open p shell. A pronounced temporal modulation in the yield of high-energy electrons is observed for C and Si, revealing a periodic spatial rearrangement of the electron density distribution in these atoms. Its period is defined by the beat between the $J = 1$ and $J = 2$ spin-orbit components of the ground state.

DOI: 10.1103/PhysRevA.88.023423 PACS number(s): 32.80.Rm, 32.80.Gc, 78.47.jm

I. INTRODUCTION

The development of femtosecond laser technology has opened up possibilities to study the ultrafast electron dynamics in atoms and molecules on a time scale of electron motion in valence shells [1–3]. The orbital alignment effect is one interesting effect that governs electron dynamics in the residual ion generated in the process of ionization of an atom in a strong laser field. The polarization of an external laser field provides a quantization axis for the electron angular momentum and its spin. The corresponding projection components m_ℓ and m_s are usually assumed to be conserved. At high laser intensities the electron tunneling rate is strongly dependent on the magnetic quantum number m_ℓ of the initial state [4,5]. For a state of nonzero angular momentum and linear polarization the ionization rates from $m_\ell = 0$ substates are typically more than an order of magnitude higher than from $m_\ell \neq 0$ substates. Therefore, the $m_\ell = 0$ orbital is primarily ionized and the residual fragment is left with a hole in the electron density distribution oriented along the laser polarization direction. This constitutes the orbital alignment effect.

Orbital alignment in laser-generated ions has received much attention in the past years. This effect was brought up to consideration by Taïeb *et al*. [6] with an attempt to describe measured photoelectron spectra [7,8] from multiple ionization of noble gas atoms in ultraintense laser pulses. Numerical simulations have shown that this effect plays an essential role in the population dynamics of multiply charged ions during the pulse, since a laser-generated ion represents an aligned target for the subsequent ionization step. However, calculations failed to reproduce the angular distributions of energetic electrons reported in Ref. [8]. The complexity of the problem was addressed with a suggestion to measure higher ionization stages reached at a given peak intensity of the laser pulse. This issue was explored by Gubbini *et al*. [9] by measuring the yields of multiply charged krypton ions as a function of laser intensity in the range of 10^{16}–10^{18} W/cm^2. Experimental results were analyzed by using the Ammosov-Delone-Krainov theory [4] and by considering separately the possibilities of fast and slow alignment relaxation. It was concluded that the relaxation is fast and at each ionization stage the photoemission rate represents a statistical average of rates from the available m_ℓ orbitals. The interaction with the magnetic component of the field and electron-electron correlations were considered as possible mechanisms causing the fast relaxation.

The role of orbital alignment in the process of sequential double detachment of atomic negative ions was discussed by van der Hart [10] on the basis of experimental results presented by Greenwood *et al*. [11]. The measured yields of singly charged positive ions, generated by double detachment, revealed a counterintuitive behavior of saturation intensities. In particular, double detachment of Ag^- was found to be more strongly saturated than double detachment of Al^-, although both the electron affinity and the ionization potential are greater in Ag than in Al. This surprising result was interpreted by van der Hart [10] by considering orbital alignment in the residual atoms generated in the first step of the sequential process and the m_ℓ dependence of the ionization rate in the second step.

While studies on multiple ionization/detachment brought contradictory results regarding the role of the alignment effect, its clear observation was performed in pump-probe experiments on strong-field ionization of Kr in a laser pulse of 10^{14}–10^{15} W/cm^2 peak intensity [12–14]. The alignment degree of the generated Kr^+ ions was measured by employing a synchrotron-based time-resolved x-ray microprobe technique. The frequency of x-ray radiation was tuned to a resonance with the $1s \rightarrow 4p$ absorption transition in Kr^+, which is absent in neutral Kr due to the filled $4p$ shell. Since x-ray absorption addresses unoccupied orbitals according to dipole selection rules, the alignment degree could be defined by measuring a difference in the x-ray absorption strength for configurations with the x-ray polarization being parallel or perpendicular to the alignment axis. It was demonstrated that the orbital alignment is preserved on a nanosecond scale and that its decay is caused by the electron-ion collisions in the ionized medium [14]. A detailed interpretation of the

*Current address: Helmholtz-Zentrum für Materialien und Energie, Albert-Einstein-Strasse 15, 12489 Berlin, Germany.

results is presented in Refs. [15,16], where the importance of spin-orbit coupling in the strong-field ionization dynamics was emphasized.

More recently, orbital alignment was shown to play an essential role in the electron dynamics induced in the ground state of the residual core by a short laser pulse [17,18]. The formation of a spatially confined hole in the electron density distribution of the valence shell is a result of coherent population of spin-orbit components of the ground state. For example, laser-generated positive ions of noble gas atoms acquire a hole in the valence p shell due to a superposition of the $p^{-1}_{j=3/2}$ and $p^{-1}_{j=1/2}$ manifolds. In order to populate these manifolds coherently, the ionization process is required to be faster than the spin-orbit period of the ground state [16]. Since the wave packet is composed of states having different energies, the created hole shows a time-dependent spatial distribution [17]. Different methods have been used to monitor the electronic motion in the laser-generated positive ions. These include the transient absorption spectroscopy with the use of isolated attosecond extreme-ultraviolet pulses [17] and the ionization-probe spectroscopy which includes measurements of the recoil momentum of the doubly charged ion and the total ionization yield [18].

We have recently developed a new method, based on angle-resolved strong-field ionization probe technique, to explore the electron dynamics in carbon atoms generated by photodetachment of their negative ions in a short laser pulse [19]. The possibility to initiate and monitor in real time electron motion in the ground state of a neutral atom represents a topic of great interest. By preparing reactive atoms with a desirable electron density distribution one can ultimately achieve control over chemical reactions. In the present work we extend our method to investigate orbital alignment and its dynamics in atoms created by photodetachment of negative ions with a half-filled valence p shell. A detailed description of the experimental method and the setup is presented.

II. METHOD

We employ a strong-field pump-probe laser scheme to investigate the time evolution of orbital alignment in laser-generated carbon, silicon, and germanium atoms. The experiment is initiated by photodetaching a valence electron from a negative ion in a strong linearly polarized laser field of short pulse duration. As discussed above, the electron emission in a strong field results in the formation of a spatially confined hole in the electron density distribution of the residual atom. This alignment is subsequently probed with a second strong laser pulse, applied at a variable time delay, which photoionizes the atom. Since the probe pulse is also strong, it ionizes the spatial portion of the electron density distribution which is oriented along its polarization axis. By employing an electron imaging technique, we project this portion onto a position-sensitive detector. This enabled us to visualize the electron density aligned along the polarization axis of the probe pulse and to monitor the motion of the electron cloud in the laser-generated atom in real time. The principle of the strong-field ionization probe technique is described in more detail below.

A. The principle of strong-field ionization probe technique

The sensitivity of strong-field ionization to the spatial distribution of the electron density in the bound state can be easily understood when the ionization process has tunneling character. In this case the valence electron leaves the core via penetrating through a potential barrier created by the superposition of the external field and the core potential. Since the potential barrier is well localized along the field polarization direction, only the fraction of the electron density which is oriented along this direction can tunnel through the barrier and consequently constitutes the ionization yield.

A similar selectivity of ionization to the electron density orientation also takes place in a multiphoton regime of this process. One can show this by using a theory based on the strong-field approximation (SFA) [20]. This theory is proven to successfully describe the processes of strong-field photodetachment and ionization [21]. Following our analysis [22] of the predictions by the SFA theory, the n-photon differential ionization rate in the laser field $\mathbf{F}(t) = \mathbf{F}\cos\omega t$ can be represented by the product of the amplitude and the interference terms (atomic units, $e = m = \hbar = 1$, are used throughout):

$$\frac{dw_n}{d\Omega} \propto \left|P_\ell^{|m|}(\sqrt{1+p^2\sin^2\theta\ /\kappa^2})\right|^2 \frac{p\ e^{-2a}}{\left|S''_{t_1}\right|^2} \times [1+(-1)^{\ell+m}\cos(b-\beta)]. \quad (1)$$

Here p is the photoelectron momentum, θ is the emission angle with respect to the laser polarization axis, $P_\ell^{|m|}$ is the Legendre polynomial, (ℓ,m) are the angular momentum quantum numbers of the electron in the initial state, $-\kappa^2/2 = E_0$ is the initial binding energy, $a = \mathrm{Im}(S_{t_1}) = \mathrm{Im}(S_{t_2})$, $b = S_{t_1} - S_{t_2}$, $\beta = 2\arg(S''_{t_1})$, and S_{t_1,t_2} are the values of the coordinate-independent part of the classical action

$$S(t) = n\omega t - \frac{\mathbf{F}\cdot\mathbf{p}}{\omega^2}\cos\omega t - \frac{F^2}{8\omega^3}\sin 2\omega t \quad (2)$$

calculated at the transition instances t_1 and t_2 that lie in the upper half-plane of complex time t and satisfy the saddle-point condition [20]

$$(\mathbf{p} + \mathbf{F}/\omega\sin\omega t_{1,2})^2 = 2E_0. \quad (3)$$

Equation (1) immediately shows that only the $m = 0$ orbital contributes to emission along the laser polarization axis, since at $\theta = 0$ the argument of the Legendre polynomial is equal to 1 and $P_\ell^{|m|}(1) = 0$ for $|m| \neq 0$. We derive below that in the limit of large number of absorbed photons, $n \gg |E_0|/\omega$, the amplitude term in Eq. (1) confines the angular distribution of photoelectrons into a narrow cone oriented along the polarization axis. Since the Legendre polynomial is multiplied by the amplitude term, the $m = 0$ contribution remains dominant in this limit.

Considering the multiphoton regime, $\kappa\omega/F \gg 1$, one can use the expansion introduced by Gribakin and Kuchiev [20],

$$c_{1,2} \simeq -i\,s_{1,2} + \frac{i}{2s_{1,2}} + O\left(s_{1,2}^{-2}\right), \quad (4)$$

where $c_{1,2} = \cos\omega t_{1,2}$, $s_{1,2} = \sin\omega t_{1,2}$, and $|s_{1,2}| \gg 1$. The latter inequality is due to the fact that the complex values

of t_1 and t_2 have a large imaginary part. Retaining only the leading terms in calculations of S_{t_1,t_2}, we obtain an expression for the amplitude term in Eq. (1),

$$\frac{p\, e^{-2a}}{\left|S''_{t_1}\right|^2} = f(\theta)\,\frac{\omega p}{2n}\left(\frac{F^2}{8\omega^3 n}\right)^n \exp\left(n+\frac{p^2}{\omega}\right), \qquad (5)$$

where the dependency on the emission angle θ is factorized as

$$f(\theta) = \frac{\exp(-p^2/\omega\sin^2\theta)}{\kappa^2 + p^2\sin^2\theta}. \qquad (6)$$

In the limit $n \gg |E_0|/\omega$ the value of $p^2/\omega \sim 2n$ is large and the exponential term in Eq. (6) dominates the angular distribution of photoelectrons. This restricts the distribution to a small angle $\Delta\theta \approx (2\ln 2/n)^{1/2}$ (FWHM), which decreases with the increase of n. For example, the emission is confined to $\Delta\theta \approx 14^\circ$ at $n = 25$ and to 10° at $n = 50$. The number of photons needed to overcome the ionization potential was disregarded in these calculations. The denominator in Eq. (6) becomes important in the limit $p^2 \gg \kappa^2$, i.e., when the electron kinetic energy is orders of magnitude larger than its initial binding energy. One can easily see that the denominator term results in an additional narrowing of the angular distribution. Such a high-energy condition, however, is not reached in the present study.

Thus, we obtain that the product of the Legendre polynomial and the amplitude term in Eq. (1) results in the selectivity of ionization to the $m = 0$ orbital and, consequently, to the electron density orientation along the polarization direction. This selectivity is stronger at higher kinetic energies, where the angular distribution of emitted electrons is narrow and forms two electron jets along the laser polarization axis [21]. By imaging the photoelectron yield in the high-energy jets we, thus, directly probe the electron density in the bound state along the laser polarization axis. In this energy range the interference term in Eq. (1) is not essential. Indeed, it was shown before that at $\theta = 0$ the interference term oscillates on the $1/p$ scale [22]. Its oscillation period is defined by the energy of the initial state and the laser frequency and is independent of the laser intensity. The first maximum of this oscillation from the side of high electron momenta defines the position of the maximum signal in the electron jet. The interference term does not oscillate within the jet and, therefore, can be disregarded in our consideration.

The high-energy jets can be easily distinguished in the angle-resolved spectra of photoelectrons, as will be demonstrated in our results. It should be noted that, under the conditions of the present experiment, the dominant ionization is in the multiphoton regime, when the nonequality $\kappa\omega/F \gg 1$ is satisfied. Despite the high peak intensity of the probe laser pulse, the main contribution to the ionization yield is defined by lower intensities due to the integration of signal over the spatiotemporal intensity distribution in the laser focus and due to the saturation effect. This matter was discussed in detail in Ref. [21].

III. EXPERIMENTAL PROCEDURE

The ion-beam apparatus used in this experiment has been described in detail elsewhere [23]. A beam of negative ions was generated using a sputter ion source. A graphite rod was used as cathode material to produce C^-, whereas powders of silicon and germanium were applied when Si^- and Ge^- ions were generated. The ion beam was accelerated to a kinetic energy of 4.5 keV and mass selected in a Wien filter. Einzel lenses, a quadrupole deflector, and deflection plates were used to steer and focus the ion beam into an electron imaging spectrometer (EIS), where it was intersected by the focused laser beams. The waist of the ion beam inside the spectrometer was approximately 1 mm and the ion current measured after the spectrometer was of the order of a few hundred nA. The pressure in the interaction region was 10^{-9} mbar.

The EIS consisted of a set of electrodes that project electrons emitted from the laser focus in the entire solid angle onto a multichannel plate detector equipped with a phosphor screen [22]. The light pulses from the screen, generated by the detected electrons, were recorded with a 1280 × 1024-pixel CCD camera. Millions of single-electron counts, accumulated during a CCD exposure time of the order of 10 min, composed a statistically significant image. In order to reduce the image distortions, the EIS was operated in the velocity mapping regime [24] with a hard projection voltage of 1.6 kV. In this regime electrons having the same momentum vector **p** were projected to the same point on the position-sensitive detector of the EIS independent of initial position in the interaction region.

Laser pulses were generated using an optical parametric amplifier (OPA) pumped with a mode-locked Ti:sapphire laser system at a repetition rate of 1 kHz. The linearly polarized idler (2055 nm) and signal (1310 nm) outputs from the OPA were used as the pump and probe beams, respectively. The long pump wavelength was chosen in order to reach a higher degree of nonlinearity of the photodetachment process. This reduced the saturation of this process at the leading edge of the pump pulse. As a consequence, the negative ions were exposed to higher laser intensities. The binding energies of C^-, Si^-, and Ge^- are 1.262 12, 1.389 52, and 1.232 71 eV, respectively [25]. At the chosen pump wavelength photodetachment of these negative ions requires absorption of at least three photons.

A schematic drawing of the optics setup is presented in Fig. 1. The signal and idler beams were split using a dichroic mirror (DM1). Their polarization axes were controlled by means of two $\lambda/2$ wave plates. The time delay between the pump and probe pulses was varied by changing the optical path length of the pump beam with the use of an optical

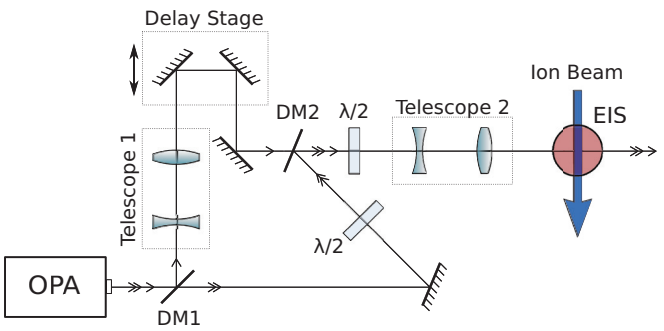

FIG. 1. (Color online) A schematic drawing of the optics setup. See text for notations.

delay stage. The divergence of the pump beam was controlled using a telescope installed in its beam path. This was used to make the focal points of the two laser beams to longitudinally coincide inside the interaction region. The two laser beams were merged using a second dichroic mirror (DM2). The merged beams were expanded and focused into the interaction region with the use of a second telescope placed in front of the experimental chamber. Diffraction-limited focal sizes of 18 μm (FWHM) and 10 μm (FWHM) for the pump and probe pulses, respectively, were measured using standard beam diagnostic tools. The pulse duration of both beams was 100 fs (FWHM). The pulse energies of the pump and probe pulses were 150 and 240 μJ, yielding the peak intensities of 8×10^{13} and 4×10^{14} W/cm^2, respectively.

Substantial efforts were made to ensure that the focuses of laser beams were on top of each other at their intersection with the ion beam. The spatial beam overlap was regularly controlled during the experiment by monitoring replicas of the focuses with a CCD camera. This was performed by inserting a glass wedge into the beam path in front of the experimental chamber, where the beam reflections from the front wedge surface were guided into the camera (not shown in Fig. 1). The larger focus size of the pump beam and saturation of the photodetachment process facilitated maintaining the condition where the probe beam interacts mainly with neutral atoms created in the aligned state. The target ions moved over a negligible fraction of the focal size during the time between the pump and probe pulses.

The zero time delay between pulses was determined by optimizing the yield of their sum-frequency generation in a thin Beta Barium Borate (BBO) crystal inserted in the beam path. The accuracy of setting the time delay to zero was of the order of 50 fs. Thereafter, the BBO crystal was removed and the delay line was adjusted to the desired time delay. All data presented in this work were acquired with time delays larger than 600 fs. This ensured that the two laser pulses were completely separated in time, hence avoiding interference between the two coherent laser pulses.

The data acquired in the experiment represented the angle- and momentum-resolved images recorded with the CCD camera of the EIS. The experimental goal was to measure the yield of high-energy electrons emitted along the polarization axis of the probe laser, as described in the previous section. Therefore, the probe polarization was kept parallel to the detector plane, enabling the required angular and momentum resolution. However, the time delay between the pump and probe laser pulses was much shorter than the time resolution of the detector. This prevented direct discrimination of electrons produced in the photodetachment step. In order to obtain an image of the photoionized electrons only, which reveals the density distribution in the aligned atom, a second image was recorded by using the pump pulse alone and subtracted from the image recorded with both pulses. The acquisition of the two images was recorded in alternating sequences of 10 s by blocking and opening the probe beam with a shutter.

The probe pulse monitors the electron density distribution along its own polarization axis, whereas the pump polarization defines the axis of orbital alignment created initially in the atom. The alignment effect was observed with a higher signal-to-background contrast by subtracting the image of ionized electrons obtained with the pump polarization being parallel to the probe polarization (the latter is fixed to be parallel to the detector plane) from the image recorded with perpendicular polarization directions. Eventually, the difference of images was normalized to their sum. The entire image processing can be represented as

$$Q = \frac{Q_\perp - Q_\parallel}{Q_\perp + Q_\parallel}, \tag{7}$$

where $Q_\perp$ and $Q_\parallel$ denote images of ionized electrons obtained with the perpendicular and parallel arrangements of the pump and probe polarizations, respectively. The signal value in the normalized image Q, averaged over a chosen range of high kinetic energies and small emission angles (see the following section), is used to quantify the alignment degree in the laser-generated atoms.

IV. RESULTS

Due to the dynamics of orbital alignment after the pump pulse, the signal distribution in the normalized image Q introduced in Eq. (7) is dependent on the time delay between the pump and the probe pulses. Therefore, it was necessary to record a sequence of images for different time delays in order to identify the area of interest in a single image, i.e., the area where the yield of high-energy electrons reveals the alignment degree in the residual atom. Figure 2 shows normalized images of ionized electrons for C, Si, and Ge averaged over different settings of the pump-probe time delays. The images represent projections of the cylindrically symmetric 3D distributions of ionized photoelectrons onto the detector plane. The symmetry axis, which is coincident with the laser polarization, is vertical in the figure. The radial distance from the image center is proportional to the electron momentum, and the coordinates $p_\parallel$ and $p_\perp$ represent the momentum components along and perpendicular to the laser polarization axis, respectively. The momentum scale was calibrated in our previous experiment [22].

Each distribution shown in Fig. 2 exhibits two opposing narrow jets along the laser polarization axis. The jets are the most pronounced in the carbon image, where they extend to electron momenta of approximately 1.5 atomic units (a.u.). This value corresponds to the absorption of more than 30 photons above the ionization threshold of C at the laser wavelength of the pump beam. Thus, the value of p^2/ω in the exponential term of Eq. (6) is large and, as follows from the analysis of this equation, the selectivity condition of ionization to the electron density distribution in the bound state is satisfied. The jets are also well pronounced in the silicon image, but to a smaller extent than for carbon. The prominence of jets is weaker in the germanium image, which immediately implies that the time-averaged alignment degree in the laser-generated Ge atom is smaller than in C and Si.

In order to reconstruct the angle- and momentum-resolved distribution of photoelectrons from a raw image recorded by the CCD camera, one needs to apply an inversion routine. A conventional Abel inversion routine based on the so-called "onion peeling" [26] was adapted in our previous studies. However, such a procedure introduces noise concentrated at the symmetry axis of the inverted image. This is in the region of

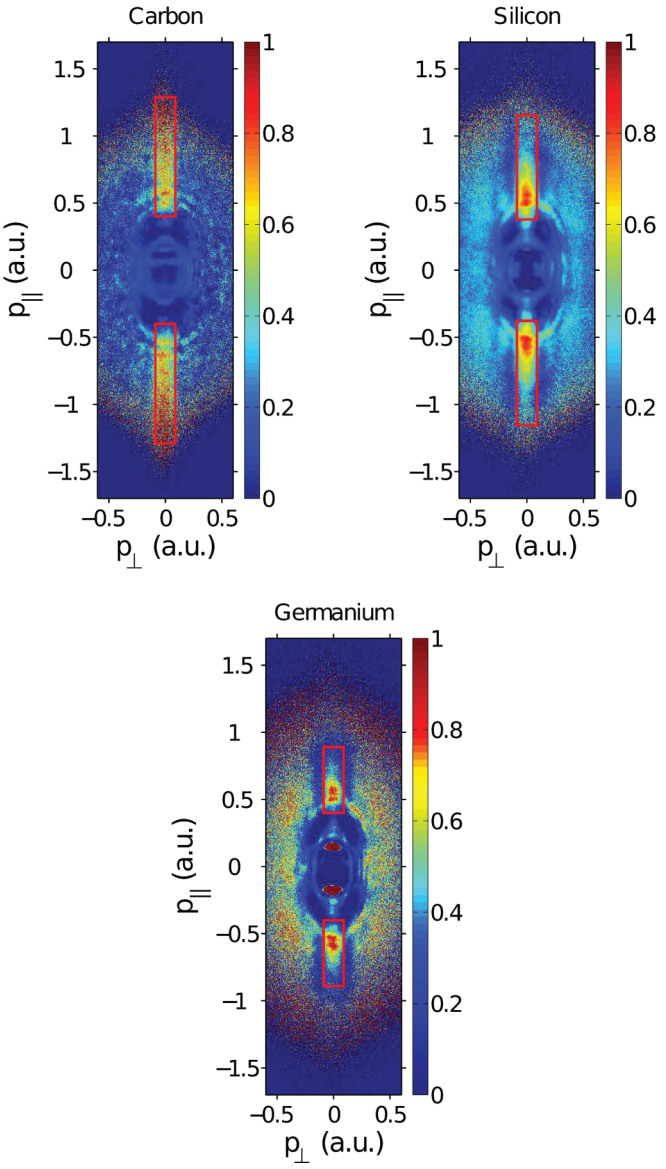

FIG. 2. (Color online) Normalized images of ionized electrons averaged over different settings of the pump-probe time delay. $p_{\parallel}$ and $p_{\perp}$ denote the electron momentum components parallel and perpendicular to the polarization axis of the probe beam, respectively. The jets of high-energy electrons are well pronounced in each image. The area of interest in the jet region used in the data analysis is outlined in red and is individually chosen for C, Si, and Ge.

small emission angles, which also is the most interesting region in the present study. We have therefore refrained from carrying out the inversion routine. Instead, the data analysis presented below involves integration of the signal in the jet regions of the noninverted images. The areas of integration, outlined in red in Fig. 2, are chosen to account for the total signal of jet electrons while avoiding the background contributions from surrounding areas. The integrated yield is used as a measure of the orbital alignment degree in the direction of the probe pulse polarization.

Figure 3 shows three representative images obtained for carbon at fixed pump-probe time delays of 2000, 2300, and 2600 fs, respectively. One should note that the normalization

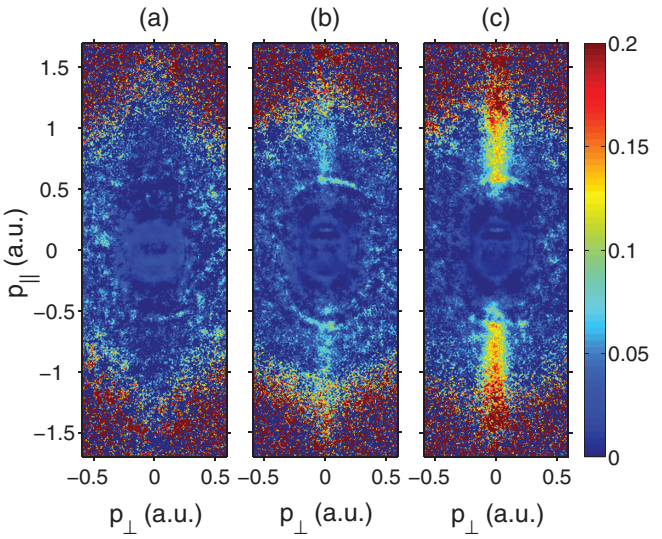

FIG. 3. (Color online) Normalized images of ionized electrons obtained for carbon at a fixed pump-probe time delay of 2000 fs (a), 2300 fs (b), and 2600 fs (c).

routine introduced in Eq. (7) improves significantly the contrast between the signal in jets and the signal in the image center, where the yield is dominated by low-energy electrons produced via photodetachment by the probe beam of negative ions that survived the pump pulse. The three chosen time delays lie within a spin-orbit period of the ground ^3P state of the C atom, which represents an intrinsic time scale of electron dynamics in this state. This matter is discussed in more detail below. The experimental results presented in Fig. 3 clearly reveal the time dependency of the electron density in the laser-generated carbon atom. Following the pump pulse, the electron hole in the valence shell of carbon starts its evolution. The hole orientation interchanges between being localized along and perpendicular to the quantization axis defined by the pump pulse polarization. Figure 3(a) represents the case where the hole is turned in the direction of the probe polarization axis and, therefore, the signal in the jet region is absent. In contrast, Fig. 3(c) shows an image where the jets are most pronounced. In this case the hole is turned at 90° with respect to the probe polarization axis and, thus, the electron density has a maximum along the direction of the probe field. Figure 3(b) represents an intermediate case.

For the quantitative analysis of the alignment dynamics in C, Si, and Ge, the ionization signal in the normalized images was integrated over the areas of interest outlined in Fig. 2. The obtained time dependencies of the integrated yield in the jet regions are shown in Fig. 4, where the time scale represents the pump-probe delay. In the carbon experiment, the time delay was varied between 600 and 5000 fs. Shorter ranges from 950 to 2200 fs and from 600 to 780 fs were investigated for Si and Ge, respectively. In each case the chosen delay range covers several spin-orbit periods of the ground ^3P state of the atom. The oscillations in the carbon and silicon data shown in Fig. 4 clearly demonstrate the dynamics of the orbital alignment initiated in these atoms by the pump pulse. One can also see that, apart from the dynamic behavior, the alignment degree

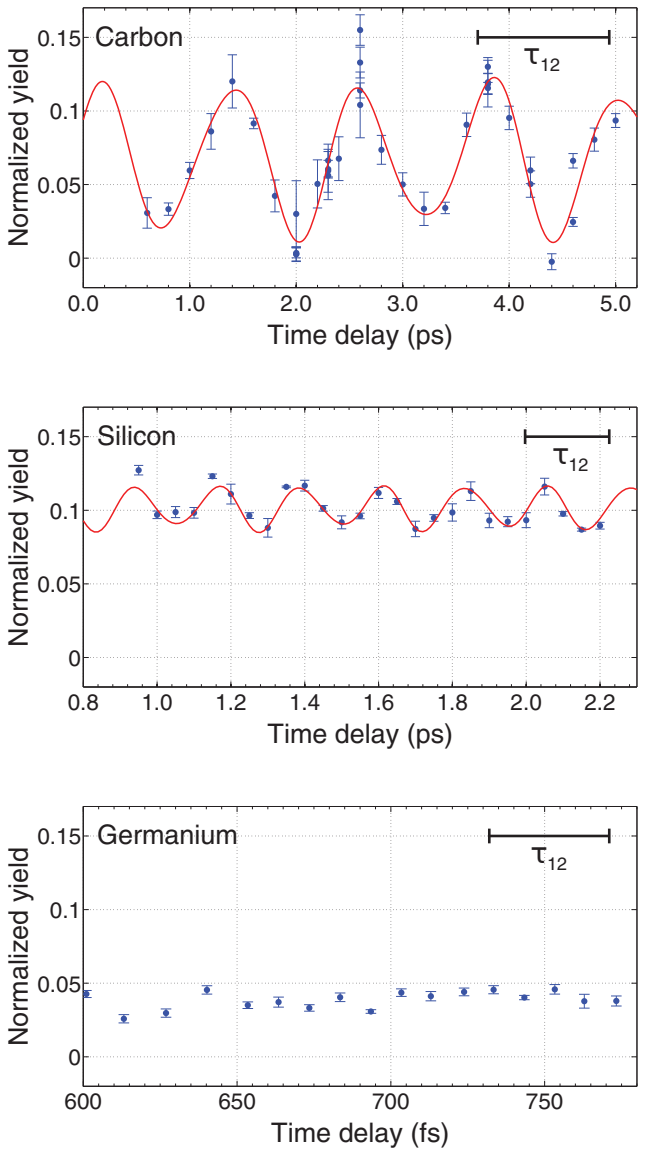

FIG. 4. (Color online) The normalized yields of high-energy electrons emitted in the ionization step plotted as a function of the time delay between the pump and the probe pulses. The yields for C, Si, and Ge are integrated over the areas of interest in the jet regions shown in Fig. 2. The solid curves represent the fit result of Eq. (8) to the experimental data. The horizontal bars depict the predicted beat periods τ_{12} between the $J = 1$ and the $J = 2$ spin-orbit sublevels of the atomic ground states.

has a constant offset. In germanium the data show a constant alignment but there is no clear sign of a temporal oscillation.

V. DATA ANALYSIS AND DISCUSSION

As pointed out in the Introduction, the alignment dynamics in the laser-generated atom manifests the time evolution of a coherently excited wave packet of atomic bound states. The three elements considered in the present work have isoelectronic p^2 configuration of the ground state, giving rise to the ^3P, ^1D, and ^1S terms [27]. Their negative ions have a p^3 $^4S_{3/2}$ electron configuration in the ground state [25]. Since spin conservation does not allow photodetachment transitions from a quartet state to a singlet state, the laser-generated C, Si, and Ge atoms can be created only in the triplet ^3P ground state. Thus, the alignment dynamics observed in carbon and silicon is due to a coherent population of the three fine-structure components of the ^3P state characterized by the total angular momentum $J = 1$, 2, and 3.

It follows that the time evolution of orbital alignment is governed by a quantum beat between three coherently excited states. The time period τ of the beat of two coherent states is given by $\tau = h/\Delta E$, where ΔE is the energy separation between the states involved and h is the Planck constant. In our case the three populated fine-structure components give rise to three possible beat periods represented by τ_{01} ($J = 0,1$), τ_{02} ($J = 0,2$), and τ_{12} ($J = 1,2$). The fine-structure energy splittings ΔE_{FS} taken from Ref. [27] and the spin-orbit (beat) periods calculated from $\tau = h/\Delta E_{FS}$ are presented in Table I. Thus, as mentioned above, a spin-orbit period of the ^3P ground state represents an intrinsic time scale of the electron dynamics in laser-generated C, Si, and Ge atoms.

Due to the three possible beat periods, a phenomenological function,

$$f(t) = c_0 + \sum_{i=1}^{3} \alpha_i \cos\left[\frac{2\pi}{\tau_i}(t - t_0)\right], \tag{8}$$

containing the sum of three harmonic functions was fitted to the data sets shown in Fig. 4, with c_0, α_i, τ_i, and t_0 being the fit parameters. Here c_0 represents a constant offset and α_i are the amplitudes of oscillations with the individual beat periods τ_i. While the time delay is measured between the maxima of the pump and probe pulses, we cannot experimentally determine the instance at the leading front of the pump pulse where the detachment process is saturated, nor the instance during the probe pulse where the ionization yield is maximum. Because of this uncertainty and the limited accuracy in the determination of the zero time delay, the fit parameter t_0 is introduced in Eq. (8).

The fit results of Eq. (8) to the data sets for C and Si are presented by the solid lines in Fig. 4, and the obtained fit parameters τ_i and α_i are given in Table I. The fit to the experimental data for Ge produced statistically nonsignificant values for the beat amplitudes (see Table I). Therefore, these results are not shown in Fig. 4 and we do not discuss them further. One can see from the amplitude parameters α in Table I that for both C and Si the alignment dynamics is dominated by the beat J_{12} between the $J = 1$ and $J = 2$ components of the ^3P state. This can be explained by considering that the multiplet levels are populated according to their statistical weights $2J + 1$ and, thus, the weights of the $J = 1$ and $J = 2$ states are the highest. The fit results reproduce well the calculated periods for the J_{12} beat in C and Si (see Table I). Considering the J_{01} and J_{02} beats, the uncertainties in the obtained amplitude values make the fit results statistically nonsignificant.

The results obtained from the fit can be verified by carrying out a Fourier analysis of the temporal dependencies shown in Fig. 4. Such an approach was already implemented by Höhr *et al.* in the study of orbital alignment in laser-generated positive ions [14]. We applied a discrete Fourier transform

TABLE I. Fine-structure splittings ΔE_{FS} [27], calculated beat periods τ_{cal}, measured beat periods τ_{exp}, and amplitudes α of the quantum beats in C, Si, and Ge. The uncertainties represent one standard deviation. The two right columns show the fit values for the constant offset c_0 and the time t_0 in Eq. (8).

	Beat	ΔE_{FS} (meV)	τ_{cal} (fs)	τ_{exp} (fs)	α (10^{-3})	c_0 (10^{-3})	t_0 (fs)
C	J_{01}	2.033	2034	1931 ± 1456	0.42 ± 2.88	67.7 ± 2.6	179.9 ± 33.8
	J_{02}	5.381	768.6	636.8 ± 22.7	3.11 ± 2.73		
	J_{12}	3.348	1235	1229 ± 17	38.5 ± 2.7		
Si	J_{01}	9.5610	432.6	410.9 ± 25.0	-1.32 ± 1.93	101.8 ± 1.4	51.4 ± 21.6
	J_{02}	27.6679	149.5	143.6 ± 2.8	1.83 ± 2.80		
	J_{12}	18.1069	228.4	222.9 ± 3.0	13.9 ± 1.9		
Ge	J_{01}	69.075 82	59.87	59.38 ± 2.88	2.22 ± 2.59	38.6 ± 1.8	-3.3 ± 30.7
	J_{02}	174.812 86	23.66	24.06 ± 1.07	-2.92 ± 3.03		
	J_{12}	105.737 04	39.11	38.81 ± 1.72	3.56 ± 2.54		

routine to the data set for Si. The obtained results are plotted in Fig. 5 as a function of the inverse Fourier frequency, $1/\nu_F$. The Fourier spectrum exhibits a distinct peak at the frequency that corresponds to the τ_{12} beat period, indicated by the arrow in the figure. All other maxima in the spectrum are caused by noise in the transform since the transform is conducted using only 26 temporal points. A larger number of experimental data points with a higher density on the time scale are needed to improve the signal-to-noise ratio in the Fourier spectrum.

The present study demonstrates a dramatic decrease in the coherence degree of orbital alignment with the increase of the fine-structure energy splitting of the ground atomic state. This result is associated with the particular laser pulse duration of 100 fs used in the experiment. Such a pulse length is approximately one order of magnitude shorter than the spin-orbit period in the ground state of carbon. Therefore, the strong temporal modulation in the ionization yield is observed in this case (see the upper part of Fig. 4), which is a result of the temporal rearrangement of the electron density distribution due to coherent population of the spin-orbit sublevels of the ground state. In contrast, no clear modulations are visible in the temporal dependency obtained for germanium (see the lower part of Fig. 4). This is because the used pulse duration is twice longer than the spin-orbit period in the ground state of germanium, which leads to noncoherent population of its fine-structure sublevels. One should note that the probe pulse duration plays an important role as well, since the ionization step period defines the time resolution in the observation of electron motion. We remind the reader at this point that the pump and probe pulses have the same length in the present experiment.

The three temporal dependencies of the ionization yield shown in Fig. 4 for C, Si, and Ge exhibit a constant positive offset, represented by the parameter c_0 in Eq. (8). It implies that the mean value of the electron density in the laser-generated atom is larger in the direction perpendicular to the pump polarization axis than in the parallel direction. This constitutes the orbital alignment effect of noncoherent character, which was observed in the experiments on strong-field ionization of noble gas atoms [12–14] and described in Refs. [15,16]. In this case population of a given spin-orbit state can be considered independently of other channels. The degree of the stationary alignment depends on the intensity-dependent admixture of photodetachment from the $m_\ell \neq 0$ substates of the negative ion, which is averaged over the spatiotemporal intensity distribution in the laser focus.

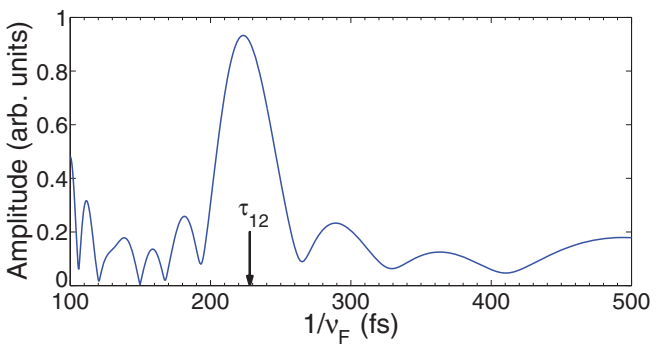

FIG. 5. (Color online) The Fourier transform of the measured time dependency of ionization yield of Si shown in Fig. 4. Note that the abscissa is inversely proportional to the Fourier frequency ν_F. The vertical arrow indicates the beat period calculated from the tabulated energy splitting of the $J = 1$ and $J = 2$ spin-orbit components of the ground state of the Si atom.

VI. SUMMARY

A strong-field pump-probe laser scheme was used to reveal the dynamics of orbital alignment in atoms generated in the process of photodetachment of their negative ions. The alignment dynamics is shown to acquire a coherent character when the time scale of the photodetachment process is shorter than the spin-orbit period of the atomic ground state. In this case the alignment effect is associated with a coherent population of spin-orbit components of the ground state. It results in a spatial confinement of the electron density distribution in the residual atom that periodically changes in time. The coherence condition was fulfilled in the experiment on C^- and Si^-, which enabled real-time observation of electron motion in the ground state of laser-generated carbon and silicon atoms. When the spin-orbit period is shorter than the time of photodetachment, the coherence condition is lost and the orbital alignment in the residual atom has a stationary character. This case was realized in the experiment on Ge^-.

Our results are in accord with the predictions by Rohringer and Santra [16], who described the alignment effect in the process of strong-field ionization of noble gas atoms.

The present work addresses orbital alignment in atoms possessing two electrons in the outer p shell. Despite the complexity of the electronic structure of these atoms, which includes three spin-orbit components of the ^3P ground state, our study reveals that only two state components of the highest statistical weight contribute significantly to the alignment dynamics. We believe that this result remains valid for atomic systems with higher multiplet orders of the ground state. Further experiments, however, are needed to verify this issue.

We have given a detailed interpretation of the strong-field ionization probe method that allows monitoring of the electron density angular distribution in bound atomic states. Its principle is based on the fact that the portion of electron density localized along the probe field polarization is mapped by the strong field to a jet of outgoing energetic electrons. The angular resolution of this method increases with the increase of kinetic energies of detected photoelectrons. The developed probe technique has a general character and is not restricted to neutral atoms. It can also be used to test angular distributions of electron densities in other (charged) atomic or molecular systems. Experiments on electron dynamics in diatomic molecules with the application of this method are in progress.

To conclude, we have developed a method to initiate and to monitor in real time electron motion in the ground state of a neutral atom. It opens a wide range of applications, where coherent control over a process can be achieved by preparing the reactive atom in its ground state with a desired electron density distribution. With the use of a laser pulse of 100 fs duration the coherence condition can be achieved in light elements, where the intrinsic time scale of electron motion lies in the picosecond range. Shorter pulses are needed to achieve coherent control in heavier atoms.

ACKNOWLEDGMENTS

The authors greatly appreciate fruitful discussions with Professor Hanspeter Helm. This work was funded by the Deutsche Forschungsgemeinschaft (DFG), Grant No. KI 865/3-1. D.H. acknowledges support by the Swedish Research council and M.E. acknowledges support by the EU-ITN Network ICONIC 238671.

[1] M. Uiberacker *et al.*, Nature (London) **446**, 627 (2007).
[2] G. Sansone *et al.*, Nature (London) **465**, 763 (2010).
[3] M. Wollenhaupt and T. Baumert, Faraday Discuss. **153**, 9 (2011).
[4] M. Ammosov, N. Delone, and V. Krainov, Sov. Phys. JETP **64**, 1191 (1986).
[5] M. V. Frolov, N. L. Manakov, E. A. Pronin, and A. F. Starace, Phys. Rev. Lett. **91**, 053003 (2003).
[6] R. Taïeb, V. Veniard, and A. Maquet, Phys. Rev. Lett. **87**, 053002 (2001).
[7] S. J. McNaught, J. P. Knauer, and D. D. Meyerhofer, Phys. Rev. Lett. **78**, 626 (1997).
[8] C. I. Moore *et al.*, Phys. Rev. Lett. **82**, 1688 (1999).
[9] E. Gubbini, U. Eichmann, M. Kalashnikov, and W. Sandner, Phys. Rev. Lett. **94**, 053602 (2005).
[10] H. W. van der Hart, Phys. Rev. A **74**, 053406 (2006).
[11] J. B. Greenwood *et al.*, J. Phys. B: At. Mol. Opt. Phys. **36**, L235 (2003).
[12] L. Young *et al.*, Phys. Rev. Lett. **97**, 083601 (2006).
[13] S. H. Southworth *et al.*, Phys. Rev. A **76**, 043421 (2007).
[14] C. Höhr *et al.*, Phys. Rev. A **75**, 011403 (2007).
[15] R. Santra, R. W. Dunford, and L. Young, Phys. Rev. A **74**, 043403 (2006).
[16] N. Rohringer and R. Santra, Phys. Rev. A **79**, 053402 (2009).
[17] E. Goulielmakis *et al.*, Nature (London) **466**, 739 (2010).
[18] A. Fleischer *et al.*, Phys. Rev. Lett. **107**, 113003 (2011).
[19] H. Hultgren, M. Eklund, D. Hanstorp, and I. Yu. Kiyan, Phys. Rev. A **87**, 031404(R) (2013).
[20] G. F. Gribakin and M. Yu. Kuchiev, Phys. Rev. A **55**, 3760 (1997).
[21] B. Bergues and I. Yu. Kiyan, Phys. Rev. Lett. **100**, 143004 (2008).
[22] B. Bergues, Z. Ansari, D. Hanstorp, and I. Yu. Kiyan, Phys. Rev. A **75**, 063415 (2007).
[23] R. Reichle, H. Helm, and I. Yu. Kiyan, Phys. Rev. A **68**, 063404 (2003).
[24] A. T. J. B. Eppink and D. H. Parker, Rev. Sci. Instrum. **68**, 3477 (1997).
[25] M. Scheer, R. C. Bilodeau, C. A. Brodie, and H. K. Haugen, Phys. Rev. A **58**, 2844 (1998).
[26] C. Bordas, F. Paulig, H. Helm, and D. L. Huestis, Rev. Sci. Instrum. **67**, 2257 (1996).
[27] A. Kramida *et al.*, *NIST Atomic Spectra Database*, version 5.0, http://physics.nist.gov/asd (2013).